Geophys. J. R. astr. Soc. (1978) **54**, 27–41

Strain-tide spectroscopy

Judah Levine* *Time and Frequency Division, National Bureau of Standards, Boulder, Colorado 80302, USA*

Received 1977 September 7

Summary. We have used two years of strain-tide data to study the response of the Earth to the diurnal and semidiurnal tidal excitations. Our results show that there is significant structure in the response of the Earth to tidal excitations near one cycle/sidereal day. This structure agrees with the resonance behaviour predicted from calculations of the forced elastic–gravitational response of an elliptical, rotating earth with a liquid outer core. The data can also be used to test for possible preferred frames and spatial anisotropies. We find that upper bounds on the parameterized post-Newtonian (PPN) parameters which characterize these effects are $\alpha_2 \lesssim 0.007$ and $\zeta_w \lesssim 0.005$. We also infer that there is a significant frequency dependence to the ocean load near one cycle/day and that the coherence between strain and barometric pressure fluctuations are significant at periods longer than a few days.

Introduction

In this paper we present an analysis of approximately two years of strain-tide data. The measurements were made using the 30-m laser strainmeter we have previously described (Levine & Hall 1972). The work was motivated in part by calculations suggesting that significant anomalies might exist in the response of the Earth to tidal excitations near one and two cycle/day.

An anomaly in the Earth tidal response to excitations near one cycle/sidereal day arises from the near degeneracy between the tidal frequencies and a free nutation mode of the Earth near one cycle/day. The mode results from the interaction of the liquid core with an elliptical, rotating mantle, and its effects on the Earth tides can be modelled as a strong frequency dependence of the effective Love numbers for the various diurnal components (Shen & Mansinha 1976). Although this effect is observable in gravity and tilt as well as in strain, it is a larger percentage of the strain tide since both gravity and tilt measurements respond directly to the applied potential as well as to the response of the Earth.

* Fellow, Joint Institute for Laboratory Astrophysics of the National Bureau of Standards and University of Colorado.

Although the exact shape of the diurnal tidal resonance produced by the near-diurnal mode is not well known, the existence of such a mode and its approximate period can be deduced from very general considerations, and there is little doubt that such a mode exists. There are other anomalies, however, whose existence is far less certain.

The interest in high-precision experiments to test gravitational theories has given rise to a theoretical framework to systematize the comparison between theory and experiment. This framework has taken the form of the parameterized post-Newtonian formalism (Will & Nordtvedt 1972). This formalism has been used to search for new tests of general relativity and to examine the viability of various theories that have been proposed as alternatives to the general theory (Nordtvedt & Will 1972).

Some theories of gravity single out a 'preferred' frame related to the mean rest frame of the Universe. These theories have recently been shown to predict observable effects related to the velocity of the solar system relative to this frame. In particular, the sidereal rotation of the Earth at frequency Ω about its axis and its orbital sidereal motion at frequency ω will produce anomalous tides at these frequencies, their harmonics, and their sums and differences. The amplitudes of these components have been calculated by Nordtvedt & Will (1972) in terms of the velocity of the Sun relative to the preferred frame, which is assumed to be the same as the velocity of the Sun relative to the centre of the Galaxy.

Warburton & Goodkind (1976) have used a superconducting gravimeter to search for these anomalous tides in the presence of classical tides at the same frequencies. They argue that the largest fractional deviation from classical theory occurs for the semidiurnal component R_2 at frequency 2Ω. Therefore if the main limitation in the measurement is assumed to come from multiplicative effects that affect the Earth tides by roughly the same percentage at all frequencies, then a measurement of the R_2 anomaly can be combined with a determination of the scalar transfer function using some other nearby component which is not perturbed by preferred frame effects to provide the most sensitive test of preferred frame theories. This technique is not optimum if, as in our case, the measurement is appreciably limited by additive noise originating either in the instrument or elsewhere. Such noise affects all components by roughly the same absolute amount, so that in this instance the most sensitive test of the existence of a preferred frame is obtained by examining the component with the largest *absolute* preferred frame effect (i.e. K_1 with a frequency of Ω). To do this we must assume that the centre frequency and the shape of the diurnal resonance are known. We shall return to this point in the discussion of results.

Data acquisition

The data used in the present work were obtained using a 30-m long laser strainmeter located in the Poorman Mine, an unworked gold mine located approximately 8 km west of Boulder, Colorado at latitude 40.03° N and longitude 254.67° E.

The heart of the strainmeter is an evacuated 30-m Fabry–Perot interferometer located along the length of the tunnel as shown in Fig. 1. The interferometer lies along an axis 7° west of north.

A block diagram of the system is shown in Fig. 2. The interferometer is illuminated by a 3.39-μm helium–neon laser using appropriate mode-matching optics. A servo loop piezoelectrically tunes the laser to keep its wavelength coincident with one of the transmission maxima of the long interferometer. The frequency of the laser is therefore related to the length of the interferometer by

$$f = \frac{nc}{2L}$$

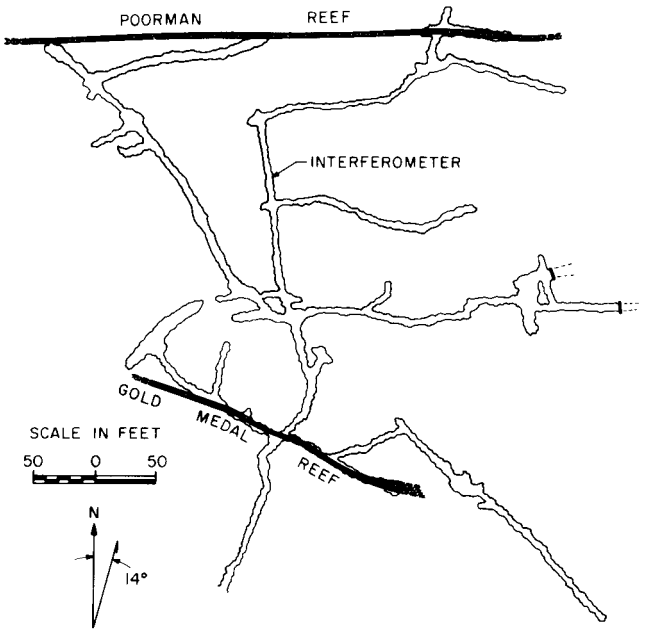

Figure 1. The Poorman Mine showing the location of the 30-m interferometer. The interferometer is approximately 60 m below ground level.

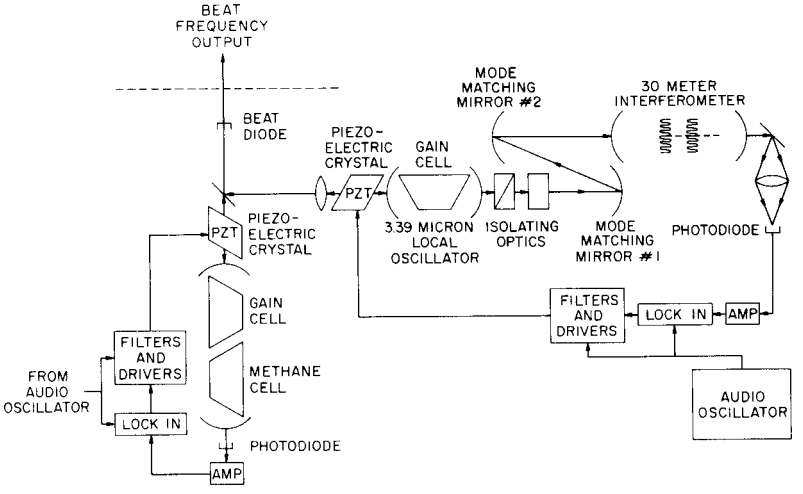

Figure 2. Block diagram of the laser strainmeter.

where n is an integer, c is the velocity of light and L is the length of the interferometer. Then

$$\frac{\Delta f}{f} = -\frac{\Delta L}{L}.$$

A second 3.39-μm laser is stabilized using saturated absorption in methane. The beat frequency between the two lasers is extracted for further processing. Thus

$$\frac{\Delta f_{\text{beat}}}{f} = \frac{\Delta L}{L}$$

or

$$\Delta f_{\text{beat}} = 8.85 \times 10^{13}\left(\frac{\Delta L}{L}\right)$$

so that a measurement of the fluctuations in the beat frequency provides a direct measurement of the fractional change in the length of the long path. The relationship between beat frequency and strain has no adjustable constants or calibration factors.

The beat frequency is processed using the apparatus shown in Fig. 3. The beat frequency is first converted to a voltage by using a precision frequency to voltage converter. The resulting voltage is then lowpass filtered, digitized and digitally recorded 10 times per hour. We have discussed the design considerations of the recording system in a previous paper (Levine & Harrison 1976).

We have incorporated several automated calibration procedures to monitor the linearity of the system and the stability of the instrumental transfer function.

The circuits shown in Fig. 3 are calibrated by injecting a series of frequencies derived from a crystal oscillator by digital division. The crystal oscillator output is phase locked to the output of a commercial rubidium vapour frequency standard. This system provides markers corresponding to strain increments of 1×10^{-8}, 2×10^{-8}, 3×10^{-8}, 4×10^{-8}, 6×10^{-8} and 12×10^{-8}. The final analog to digital converter is calibrated by sampling the system ground (to establish the zero) and the voltage output of a voltage standard to establish the gain.

The linearity of the system is monitored by modulating the length of the 30-m interferometer using a piezoelectric crystal mounted in the mirror mount for that purpose. The linearity of the system is investigated by applying a square wave with a period of 10 hr to the crystal. Any non-linearity in the system shows up as a beat between the tides and the calibration signal which produces a spurious strain signal at 1.4 cycle/day. This frequency lies well away from all of the tidal components and is in a quiet region of the spectrum.

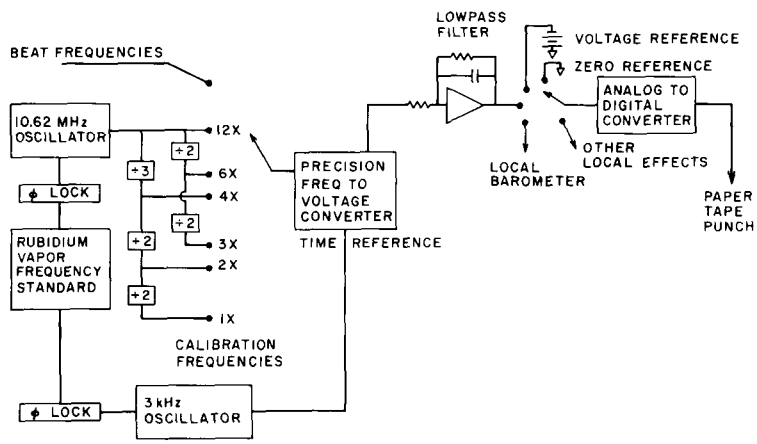

Figure 3. Recording and calibration system.

The various calibration procedures are performed at different intervals. The final analog to digital converter is calibrated 10 times per hour every time a data point is recorded. The calibration becomes part of the data record and provides a continuous check of the system. The frequency markers are inserted into the system at a different time every day to minimize the possibility of masking a nearly diurnal effect. The square-wave linearity check is performed once a month.

Fig. 4 shows the change in the relative calibration during the experiment. A calibration factor of unity was arbitrarily assigned to the midpoint of the data set. The long-term drift in the calibration comes mostly from the ageing of capacitors in the lowpass filter and from a slow change in the offset of the analog to digital converter. In Fig. 5 we present the calibration data in a form that is more significant in the current work. We have plotted the relative calibration as a function of the local time to see if the calibration factor had a diurnal or semidiurnal fluctuation. The bars at each point represent the range of calibrations recorded at that time, and the point plotted is the mean of the observations. The straight line is a least-squares fit to the data. Its slope is zero and the residuals of the fit are randomly distributed. We conclude that the system has no measurable sensitivity to local thermal or barometric pressure fluctuations at either one or two cycle/day.

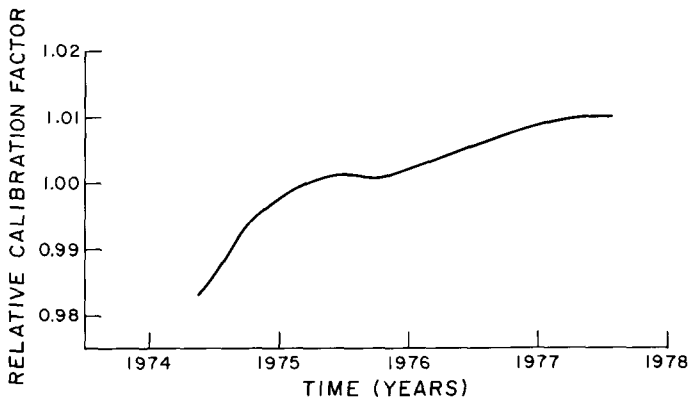

Figure 4. Time dependence of the calibration factor. The calibration factor is shown relative to its value in early 1975.

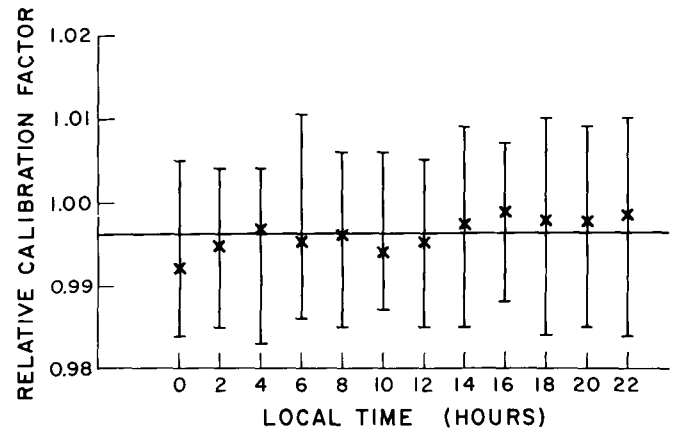

Figure 5. The calibration factor shown as a function of the local civil time. For each point the bars represent the range of values recorded and the cross marks the average of all of the values recorded at that time.

The results of the square-wave linearity test are also negative. We conclude that if a non-linear effect is present its effect puts less than one part in a thousand of the input signal into the difference frequency sideband. At this level, a non-linear effect cannot be distinguished from purely statistical fluctuations in the background noise.

Data reduction

The data analysed in this paper cover a period of about 980 days starting on 1974 May 21.

The first step in the data-reduction process was to fill in the gaps due to instrumental failure. These gaps average 10 hours in length and occur on the average of once per month. To fill in the gaps we use a time series derived from a least-squares analysis of the data immediately adjacent to the break. The process has been described previously (Levine & Harrison 1976) and it results in a patch which does not introduce discontinuities in the data set.

The second step in the data-reduction process was to remove changes in the baseline having Fourier components in the tidal bands. These changes are produced by local effects (mostly large changes in the barometric pressure). They cannot be removed by simple digital or analog filtering since they have appreciable energy in the tidal-frequency bands. Failure to remove them introduces a significant bias into the subsequent analysis since they introduce phase-modulation sidebands in the tidal spectrum. The resulting sidebands produce spurious effects including 'non-linearities' reported earlier (Levine & Harrison 1976).

We have dealt with these baseline steps by the following procedure: we break the data into consecutive 48 hour blocks. We fit a diurnal and a semidiurnal wave to each block using four adjustable parameters (two amplitudes and two phases). The residuals of this fitting procedure are computed. The residuals are smoothed by lowpass filtering using a convolution filter with symmetrical lead and lag weights. This procedure produces a time series which contains essentially no tidal energy, but which faithfully reflects changes in the baseline even as large as a third of a tidal amplitude in a day (changes of this magnitude are often produced when a storm front moves into the area). The smoothed residuals are subtracted from the data set point by point to yield the final data (A. Szoke 1975, private communication).

We have conducted extensive tests of this procedure. In Appendix A we show an example of the use of this procedure. The 48-hr block length is long enough to allow unambiguous separation of true tidal signals from changes in the baseline, while at the same time being short enough so that a simple two-frequency fit can extract all of the tidal energy. The process is intuitively appealing in that it deals with baseline changes in the time domain where they are well characterized as local perturbations rather than in the frequency domain where they are not well characterized and where their energy is spread over a broad spectrum – often appearing as spurious phase-modulation sidebands of the principal tidal frequencies.

Following this procedure the data are bandpass filtered using a symmetric convolution filter and then decimated to one sample every two hours for comparison with theory.

Tide theory

The strain tide at a given station is calculated from the tidal potential in a straightforward manner (Melchior 1966). The calculation of the potential is considerably more difficult.

The tidal anomalies that we are studying produce anomalous amplitudes at certain classical tidal frequencies. It is therefore not sufficient to characterize a certain tidal theory in terms of its predictive power for the total time series or even in terms of the rms deviation

of the calculated series from the 'true' tides. We must be concerned with the spectrum of the deviations to be sure that large errors do not exist in the calculation of small components, and that the spectrum of the deviations is relatively flat. Thus a tidal theory that calculates the lunar position by arbitrary truncation of the Fourier expansion of the lunar motion will have errors that are obviously not randomly distributed. We have conducted tests of various tide-generating algorithms (Munk & Cartwright 1966) which confirm our general conclusion, namely that the tidal time series does not differ significantly from the 'true' tides (the disagreement often being less than 1 per cent in the time series), but the amplitudes of many of the smaller components are wrong.

We have used two independent methods for calculating the astronomical input for the Earth-tide calculations. Our primary calculations were done using the results of Cartwright & Taylor (1971) and Cartwright & Edden (1973). These amplitudes are compared with a direct calculation using the Jet Propulsion Laboratory ephemeris DE-96 (Newhall 1976). We did not find any significant errors in our spot check of the Cartwright & Edden tables (approximately 10 per cent of the amplitudes were checked) and so we have used them in all of our calculations.

Data analysis

We have used all of the diurnal and semidiurnal components published by Cartwright & Edden in our analysis. For each component we construct a times series in the form:

$$a_K \cos(2\pi f_K t + \Phi_K + \alpha_K)$$

where a_K is the amplitude given by Cartwright & Edden, f_K is the frequency (in cycle/hr) evaluated from the Doodson number of the component (whose six digits are $I_1, I_2 \ldots I_6$):

$$\begin{aligned} f_K = {} & 4.025570033 \times 10^{-2}\, I_1 + 1.525045888 \times 10^{-3}\, (I_2 - 5) \\ & + 1.140795542 \times 10^{-4}\, (I_3 - 5) + 1.289400833 \times 10^{-5}\, (I_4 - 5) \\ & + 6.128929167 \times 10^{-6}\, (I_5 - 5) + 5.45 \times 10^{-9}\, (I_6 - 5). \end{aligned}$$

Φ_K is the phase (in degrees) at the start of the analysis epoch, t_0,

$$\begin{aligned} \phi_K = {} & 217.89822\, I_1 + 22.22101\, (I_2 - 5) + 60.11923\, (I_3 - 5) \\ & + 271.56503\, (I_4 - 5) + 188.82048\, (I_5 - 5) + 282.25919\, (I_6 - 5) \\ & + 360 f_K (t_0 - 529356), \end{aligned}$$

and α_K is $-90°$ if the term arises from a spherical harmonic Y_n^m in which $(n+m)$ is odd and is zero otherwise (Cartwright & Taylor 1971). The quantity t is the number of hours from the start of the data set, while t_0 is the elapsed time from 1900.0 to the start of the data set (in our current analysis t_0 = 652047.9). Each term is then multiplied by the appropriate spherical harmonic of the station colatitude θ and east longitude ϕ, and by an algebraic function of the station coordinates and the strainmeter orientation θ_s (measured in degrees clockwise from north):

$$a_K \cos(2\pi f_K t + \Phi_K + \alpha_K)\, Y_n^m(\theta, \phi)\, T(n, m, \theta, \phi, \theta_s)$$

where Y_n^m is the normalized spherical harmonic and T is a function converting potential to strain (Levine & Harrison 1976). In addition to the explicit dependences stated, T depends in a complicated way on the Love numbers h and l. Our initial calculations were done using the values of h_n and l_n given by Longman (1963). The theoretical series were further modified by a function to correct for local topography, local crustal inhomogeneities, cavity effects

and ocean loads. We assumed initially that these effects do not vary rapidly with frequency, that all of the diurnal components have the same correction as O_1, and that all of the semidiurnal components have the same correction as M_2. These corrections appear as an amplitude correction $B(m)$ and a phase shift β_m so that the theoretical series is of the form:

$$d_K = B(m)a_K \cos(2\pi f_K t + \Phi_K + \alpha_K - \beta_m)\, Y_n^m(\theta, \phi) T(n, m, \theta, \phi, \theta_s).$$

For purposes of subsequent analysis we also construct a quadrature series:

$$e_K = B(m)a_K \sin(2\pi f_K t + \Phi_K + \alpha_K - \beta_m)\, Y_n^m(\theta, \phi)\, T(n, m, \theta, \phi, \theta_s).$$

Both physical intuition and mathematical stability argue that it is unwise to fit these terms to the data directly. Many of the terms cannot be separated with only two years of data. In addition there is almost no basis for postulating appreciable structure in the transfer function at a resolution of order one cycle/decade. We therefore form the summed time series

$$D_{K'} = \sum_K d_K$$

and

$$E_{K'} = \sum_K e_K$$

where each term of $D_{K'}$ contains the sum of all terms d_K (regardless of parentage) having frequencies which differ by less than one cycle/yr from each other. The terms $E_{K'}$ are formed in a similar way from e_K. This process reduces the number of series to be fit from 329 pairs of d_k and e_K to 48 pairs of $D_{K'}$ and $E_{K'}$. In addition to these time series we included a time series of barometric pressure readings obtained at the mine. These series were fit to the data with amplitudes that were adjusted for a best fit in a least-squares sense. This procedure results in a normalized transfer function with two degrees of freedom

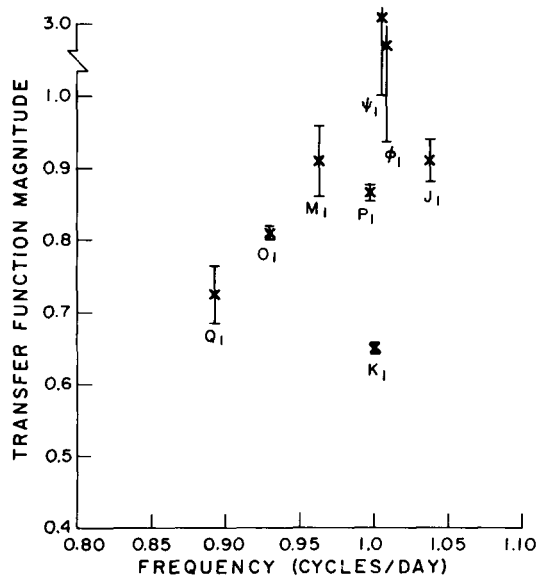

Figure 6. Normalized transfer-function amplitude for the diurnal tides. For clarity only the major components are plotted. The error bars are one standard deviation.

in each cycle/yr wide frequency band. The transfer function amplitude for the diurnal tidal band is plotted in Fig. 6 and the phase is plotted in Fig. 7. The corresponding quantities for the semidiurnal band are plotted in Fig. 8.

The error bars represent one standard deviation and are obtained from estimates of the noise. They do not include any possible systematic effects.

We have estimated the noise in two different ways. We first assumed that there is no fine structure in the noise spectrum and that frequencies one or two cycle/yr apart have essentially the same noise power. We can then estimate the noise at tidal frequencies by measuring the power in adjacent frequency bands containing no tidal energy. This estimate yields a noise power of approximately 30×10^{-22} (strain)^2/(cycle/yr), a value essentially

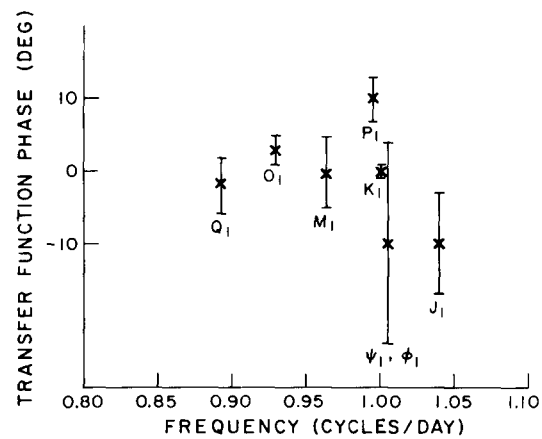

Figure 7. Normalized transfer-function phase for the diurnal tides. For clarity only the major components are plotted. The error bars are one standard deviation.

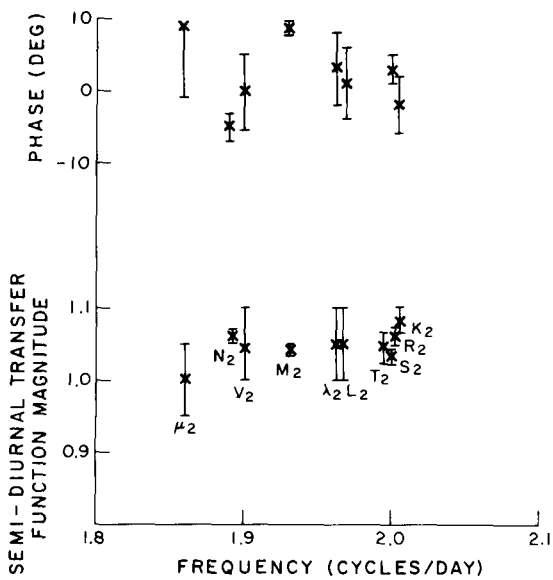

Figure 8. Normalized transfer-function amplitude (lower curve) and phase (upper curve) for the semidiurnal tides. For clarity only the major components are plotted. The error bars are one standard deviation.

equal to our previously published broadband-noise estimates (Berger & Levine 1974). The second method involves examining the residual power at tidal frequencies after the least-squares fit has been subtracted from the original data. This process yields the same noise-power estimate as above, suggesting that all of the excess power at tidal frequencies is coherent with the primary tides, and that the linear model we have used in our analysis completely explains the data. Furthermore, since the power spectrum of the residuals is essentially identical to our previous published broadband estimate (Berger & Levine 1974), we conclude that there are no additional narrowband sources of strain excitation other than the tides and the barometer (the only exception is a strong thermo-elastic effect at S_1 to be discussed below).

Our least-squares fitting procedure also yields a statistically significant dependence of measured strain on local barometric pressure, although it does not provide any information on the frequency dependence (if any) of the admittance to barometric pressure.

The frequency dependence may be calculated by computing the coherence between barometric pressure and strain. We divide the two time series into consecutive blocks of equal length and we then compute the Fourier transforms of each block. Then if $A_j(\omega)$ is the Fourier component at frequency ω for the jth block of one series and $B_j(\omega)$ is the corresponding quantity for the other series, the coherence is defined as

$$\gamma_{ab}(\omega) = \left\{ \frac{|\langle A_j(\omega) B_j^*(\omega) \rangle|^2}{\langle |A_j(\omega)|^2 \rangle \langle |B_j(\omega)|^2 \rangle} \right\}^{1/2}$$

where averages are taken over all of the blocks. In Fig. 9 we show $\gamma_{ab}(\omega)$ as a function of frequency. Note that the coherence is high at low frequencies, but that it drops to statistically insignificant values at one cycle/day and above. Thus the barometric pressure has very little effect on our tidal data although it is responsible for a significant fraction of the long period (periods on the order of one week) noise.

Discussion of results

The amplitude of the diurnal transfer function shows a statistically significant structure. There appears to be a significant decrease in the transfer function for the low-frequency diurnal components. We attribute this to a slow change in the contribution of the ocean load to our observed data.

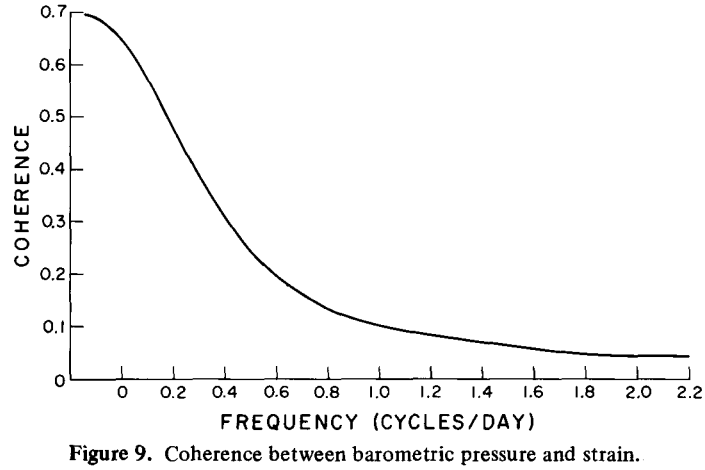

Figure 9. Coherence between barometric pressure and strain.

More significantly there is a dip in the transfer function near one cycle/day (we have not plotted the S_1 amplitude at one cycle/day since it is heavily contaminated by thermoelastic processes). This dip is consistent with the effects of the nearly diurnal resonance associated with the liquid core. The consistency can be shown more clearly by inserting the resonance directly into the fitting function by using the frequency dependent Love numbers published by Molodensky (1961) and by Shen & Mansinha (1976). These Love numbers produce changes in the transfer function at all of the diurnal frequencies but, except near one cycle/day, the new transfer function lies within the one standard deviation error bars of the old one. The modified transfer function is shown in Fig. 10. As can be seen from the figure the resonance models account for the dip in the transfer function near one cycle/day. Unfortunately, the data cannot be used to infer the fine structure near the resonance. Furthermore, the insertion of realistic estimates for the energy loss in the nearly diurnal mode may affect all of the models somewhat. It is unlikely that we will be able to test any of these effects using our data. The strongest test for the resonance obtainable from our data comes from the components P_1 and K_1 which are really on the tail of the resonance function. Our measurements at ϕ_1 and ψ_1 (where the resonance has the largest effect) have error bars whose size probably does not permit them to be used in a quantitative comparison between theory and experiment or in attempts to differentiate among the various calculations of the effect of the resonance.

These results may be compared with the analysis of Warburton & Goodkind (1976, 1977) using data from a cryogenic gravimeter, with the gravimeter data analysis of Abours & Lecolazet (1977) and with the analyses of Lecolazet & Melchior (1977). Their results are generally in agreement with ours in confirming the general shape of the resonance. None of the analyses is able to make a quantitative comparison with theory because of the relatively poor signal to noise ratio in the measurements of the crucial components ψ_1 and ϕ_1. Except for Warburton & Goodkind none of the groups has published detailed analyses of the residuals of the fit.

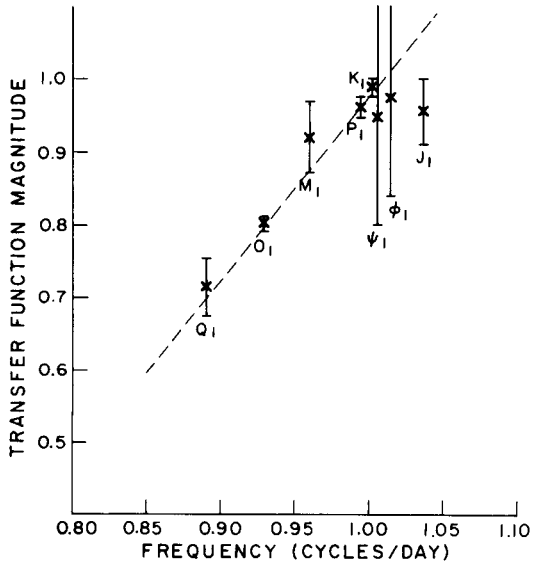

Figure 10. Normalized transfer-function amplitude for the diurnal tides when the frequency-dependent Love numbers are inserted into the fitting function. The dashed line is obtained by fitting a straight line to the transfer-function amplitudes weighted by their respective uncertainties.

The semidiurnal transfer-function amplitude shows far less structure, and the agreement between experiment and theory is good (i.e. the transfer-function magnitude is close to unity). There is no evidence of anomaly at S_2 (two cycle/day) confirming that the anomaly at S_1 is almost certainly of thermo-elastic origin. There is no evidence of an anomaly at R_2, the component which would be affected by the existence of a preferred frame effect.

We may place upper limits on the various PPN parameters by calculating the magnitudes of the anomalous tidal components in terms of the PPN parameters α_2 and ζ_w. These anomalous effects appear as additional terms in the applied potentials, so that we may use the machinery we have already developed for calculating the strain.

The measured strain is related to the applied potential by the quantities $T(n, m, \theta, \phi, \theta_s)$ used above and defined previously. The value of T at our station ($\theta = 49.97°, \phi = 254.67°$) is approximately 0.17 for diurnal tides and 0.35 for semidiurnal tides. The response of a gravity meter is approximately 1.18 times the applied potential in the same units so that the strainmeter provides a weaker test of these effects.

We feel that our measurements of the transfer function near one and two cycle/day are consistent with the hypothesis that the ocean load is a smoothly varying function of frequency over the narrow range of frequencies near one and two cycle/day. With this assumption the most sensitive test for a non-zero value of the PPN parameter α_2 comes from an examination of K_1 (the component with the largest anomalous tide) relative to O_1 and P_1. We conclude that the anomalous strain amplitude at K_1 does not exceed 1.5×10^{-10}. The anomalous tide has an amplitude of approximately $210 \times 10^{-10}\ \alpha_2$ so that $\alpha_2 \lesssim 0.007$. If we do not assume that the diurnal core resonance is sufficiently well known to permit the use of K_1, we obtain a somewhat weaker test using the semidiurnal component, R_2. We find $\alpha_2 \lesssim 0.01$.

We estimate an upper bound to the anisotropy parameter ζ_w in the same way. The amplitude of the anomalous tide at one cycle/sidereal day is $3 \times 10^{-8}\ \zeta_w$ while the amplitude at two cycle/sidereal day is $2.5 \times 10^{-8}\ \zeta_w$. Thus the diurnal test yields $\zeta_w \lesssim 0.005$ while the semidiurnal test yields a somewhat larger upper bound ($\zeta_w \lesssim 0.007$).

Conclusions

We have analysed two years of strain-tide data using a method which we feel has several advantages over conventional Fourier methods or least-squares fitting of spherical harmonics with optional leads/lags (Munk & Cartwright 1966). Our method has all the advantages of time-domain analysis: the ability to fit non-harmonic series (e.g. barometric pressure) and the reduction in the contamination of weak lines by nearby strong ones. At the same time it has the advantage of Fourier methods in that it is straighforward to interpret the results, is numerically stable, and is well suited for investigating anomalies characterized in the frequency domain since it yields the frequency dependence of the tidal admittance directly.

Our analysis shows that there is a significant anomaly in the strain tide transfer function near one cycle/day, and that the anomaly is removed by using the frequency-dependent Love numbers calculated to result from the existence of a resonance due to the liquid outer core. We are unable to differentiate among the various effects of the resonance because of the uncertainties in our determination of the amplitudes of the tides at ψ_1 and ϕ_1.

The amplitude of the transfer function shows a nearly linear dependence across the diurnal band. As shown by the dotted line in Fig. 10, the amplitudes of all of the components except J_1, lie less than one standard deviation away from a straight line with a slope of 2.41/cycle/day. The amplitude of J_1 is approximately two standard deviations below this line. The scatter of the points about the line shows no clear systematic trend and we do not feel that the data are better fitted by a higher-order polynomial. A sinusoidally varying

function does not fit the data quite as well and such a fit deviates significantly from the measured values at P_1 and K_1.

Our data also yield upper bounds on the PPN parameters α_2 and ζ_w which measure the existence of a preferred frame or a spatial anisotropy, respectively. In these experiments we are less sensitive than a gravity meter would be by about a factor of six. Our upper limits ($\alpha_2 \lesssim 0.007$, $\phi_w \leq 0.005$) exceed those of Warburton & Goodkind (1976) (who used data from a superconducting gravity meter) by roughly this factor of six. It is important to note that the limitations on the measurements are not due to the instrument in either case but result from various random fluctuations in the Earth and the atmosphere which affect both measurements and which are not totally removed by the algorithms used to date.

The analysis of gravimeter data is complicated by the non-negligible sensitivity of the measurement to fluctuations in barometric pressure. One must be concerned about possible uncertainties or changes in the barometric pressure admittance. Furthermore the data of Abours & Lecolazet (1977) show that the barometric pressure admittance is neither very well known nor independent of frequency.

It is also possible for the calibration constant of the gravimeter to change with time, although this could be detected by periodic recalibration.

The analysis of the strainmeter data is made more difficult by the sensitivity of the instrument to local topography and crustal inhomogeneities and by the fact that the inherent signal to noise ratio is poorer for strain tides than for gravity tides. This effect is not totally compensated for by the fact that phenomena such as the nearly diurnal-core resonance produce larger fractional effects in strain tides.

Acknowledgments

We gratefully acknowledge the many helpful discussions we have had with A. Szöke during his tenure as a Visiting Fellow at JILA and with P. L. Bender.

References

Abours, S. & Lecolazet, R., 1977. New results about the dynamical effects of the liquid outer core, as observed at Strasburg, *Proc. 8th Int. Conf. Earth tides,* in press.

Berger, J. & Levine, J., 1974. The spectrum of the Earth noise from 10^{-8} to 10^{+2} Hz, *J. geophys. Res.*, **79**, 1210–1214.

Cartwright, D. E. & Edden, A. C., 1973. Corrected tables of tidal harmonics, *Geophys. J. R. astr. Soc.*, **33**, 253–264.

Cartwright, D. E. & Tayler, R. J. 1971. New computations of the tide-generating potential, *Geophys. J. R. astr. Soc.*, **23**, 45–74.

Lecolazet, R. & Melchior, P., 1977. Experimental determination of the dynamical effects of the liquid core of the Earth, *Ann. Geophys.*, **33**, 11–22.

Levine, J. & Hall, J. L. 1972. Design and operation of a methane absorption stabilized laser strainmeter, *J. geophys. Res.*, 77, 2595–2609.

Levine, J. & Harrison, J. C., 1976. Earth tide strain measurements in the Poorman Mine near Boulder, Colorado, *J. geophys. Res.*, **81**, 2543–2555.

Longman, I. M., 1963. A Green's function for determining the deformation of the Earth under surface mass loads. II. Computation and numerical results, *J. geophys. Res.*, 68, 485–496.

Melchior, P., 1966. *The Earth tides,* Pergamon Press, Oxford.

Molodensky, M. S., 1961. The theory of nutations and diurnal Earth tides, *Comm. Obs. R. Belgique,* **188**, 25–56.

Munk, W. H. & Cartwright, D. C., 1966. Tidal spectroscopy and prediction, *Proc. R. Soc. Lond. A,* **259**, 533–581.

Newhall, S., 1976. *JPL export ephemeris, DE-96,* Jet Propulsion Laboratory, Pasadena, California.

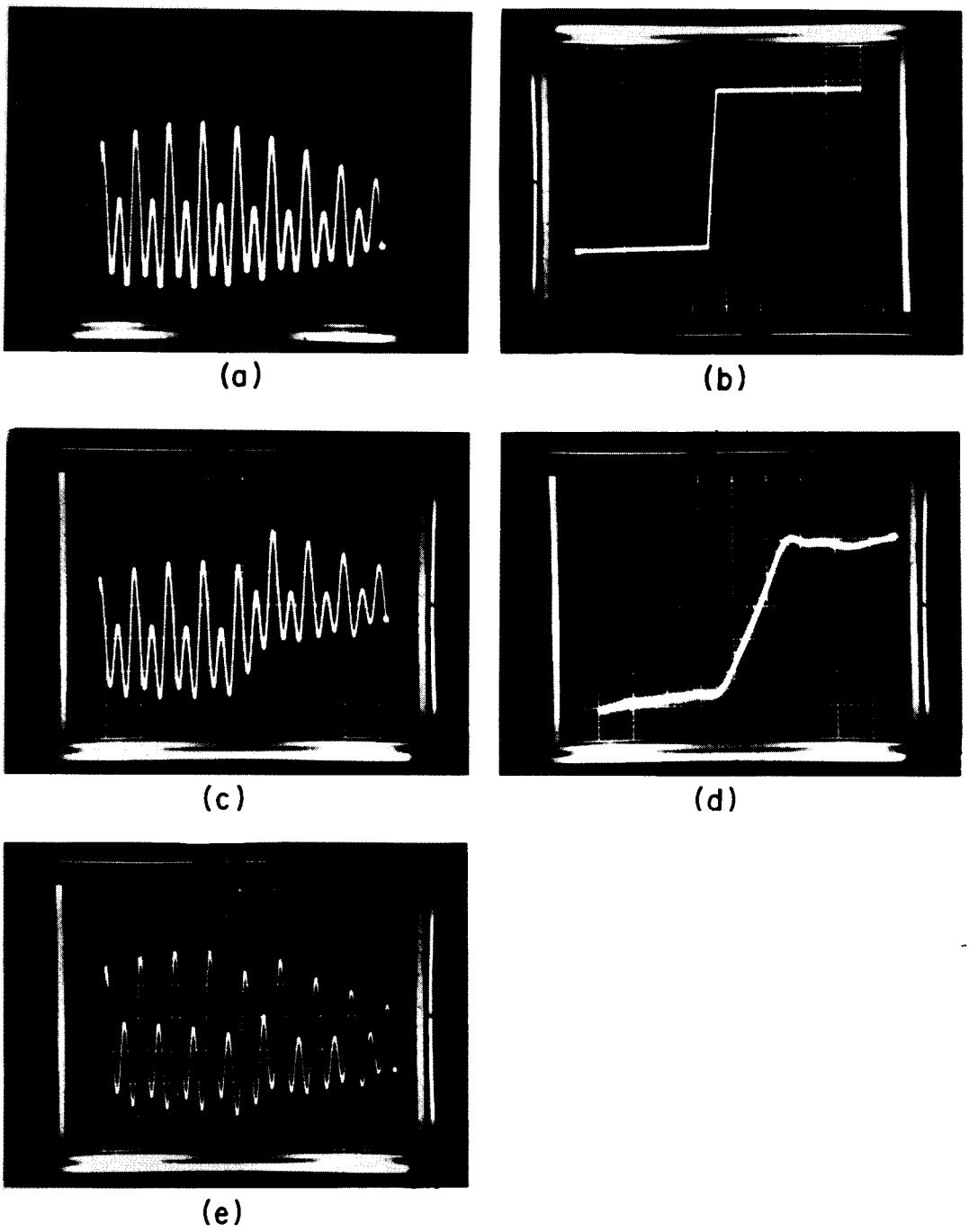

Figure 11. (a) Theoretical strain-tides series computed using the latitude, longitude and azimuth of the Poorman Mine instrument. The series is 204.8 hr long and the tide is computed every 0.1 hr. Vertical scale is 1.08×10^{-8} / division. (b) Synthetic baseline. The function is zero for the first 105 hr (1050 points), rises linearly at a rate of 2×10^{-9} /hr for 8 hr and is then constant. (c) The point by point sum of the data sets shown in (a) and (b). The vertical scale is 1.3×10^{-8} /division. (d) The smoothed residuals of the fitting procedure. (e) The point by point difference of the data sets shown in (c) and (d). The vertical scale is 1.12×10^{-8} /division.

Nordtvedt, K. Jr. & Will, C. M., 1972. Conservation laws and preferred frames in relativistic gravity. II. Experimental evidence to rule out preferred theories of gravity, *Astrophys. J.*, 177, 775–792.

Shen, Po-Yu & Mansinha, L., 1976. Oscillation nutation and wobble of an elliptical rotating earth with liquid outer core, *Geophys. J. R. astr. Soc.*, 46, 467–496.

Warburton, R. J. & Goodkind, J. M., 1976. Search for a preferred reference frame, *Astrophys. J.*, 208, 881–86.

Warburton, R. J. & Goodkind, J. M., 1977. Detailed gravity tide spectrum between 1 and 4 cycles per day, *Geophys. J. astr. Soc.*, 52, 117.

Will, C. M. & Nordtvedt, K. Jr., 1972. Conservation laws and preferred frames in relativistic gravity. I. Preferred-frame theories and an extended PPN formalism, *Astrophys. J.*, 177, 757–774.

Appendix A: example of the procedure for removing fluctuations in the baseline

In order to test our procedure for removing relatively rapid changes in the baseline, we have used the strain-tide series shown in Fig. 11(a). To this series we added the baseline shown in Fig. 11(b). It is zero for the first 105 hours of the record, rises linearly at a rate of 2×10^{-9}/hr for 8 hours and is then constant for the remainder of the record. The resultant sum is shown in Fig. 11(c).

Using the procedure outlined in the text, we fit the data of Fig. 11(c) with a diurnal and a semidiurnal wave in each 48-hr block. The smoothed residuals of this fit are shown in Fig. 11(d). Note the effect of the symmetric lead/lag filter. Fig. 11(e) is obtained by subtracting the residuals of (d) from the data of (c).

We may characterize the effectiveness of the procedure by computing the amplitudes of the various data sets at the major tidal frequencies (O_1, and M_2). The results are shown in Table A1, normalized to the respective amplitudes of the original data.

The diurnal components are more heavily affected, but the procedure substantially reduces the discrepancy with the original data set from 26 to just over 4 per cent.

Table A1. Fourier transform of the data before and after baseline removal (normalized to Col. 1).

	Original data	Data with step	Step removed
Diurnal amplitude (O_1)	1	0.74	0.96
Semidiurnal amplitude (M_2)	1	0.94	0.99